

Resolving phase stability in the Ti-O binary with first-principles statistical mechanics methods

N. S. Harsha Gunda,¹ Brian Puchala,² and Anton Van der Ven^{1,*}¹Materials Department, University of California Santa Barbara, Santa Barbara, California 93106, USA²Materials Science and Engineering Department, University of Michigan, Ann Arbor, Michigan 48109, USA

(Received 25 September 2017; published 30 March 2018)

The Ti-O system consists of a multitude of stable and metastable oxides that are used in wide ranging applications. In this work we investigate phase stability in the Ti-O binary from first principles. We perform a systematic search for ground state structures as a function of oxygen concentration by considering oxygen-vacancy and/or titanium-vacancy orderings over four parent crystal structures: (i) hcp Ti, (ii) ω -Ti, (iii) rocksalt, and (iv) hcp oxygen containing interstitial titanium. We explore phase stability at finite temperature using cluster expansion Hamiltonians and Monte Carlo simulations. The calculations predict a high oxygen solubility in hcp Ti and the stability of suboxide phases that undergo order-disorder transitions upon heating. Vacancy ordered rocksalt phases are also predicted at low temperature that disorder to form an extended solid solution at high temperatures. Predicted stable and metastable phase diagrams are qualitatively consistent with experimental observations, however, important discrepancies are revealed between first-principles density functional theory predictions of phase stability and the current understanding of phase stability in this system.

DOI: [10.1103/PhysRevMaterials.2.033604](https://doi.org/10.1103/PhysRevMaterials.2.033604)

I. INTRODUCTION

Titanium is a highly reactive element and forms a rich variety of compounds and solid solutions with elements such as oxygen [1,2], nitrogen [3], carbon [4], and boron [5]. The Ti-O binary in particular consists of a wide variety of stable and metastable oxides and suboxides [1]. These include the rutile, anatase, brookite, and bronze-B polymorphs of TiO₂, the family of TiO_{2n-1} Magnéli phases, corundum Ti₂O₃, a vacancy containing rocksalt form of TiO, and hcp based TiO_x suboxides. The list of suboxides was recently expanded after the synthesis of a new polymorph of TiO having an ω -Ti sublattice with oxygen filling a subset of its interstitial sites [6].

The oxides of Ti are used in many wide-ranging applications. The various polymorphs of TiO₂, for example, are actively studied as electrodes for Li and Na-ion batteries and for photocatalytic applications [7–19]. Many of the oxides in the Ti-O binary form as part of a multilayer oxide scale as Ti and its alloys are exposed to oxygen rich environments. Each oxide polymorph has very distinct properties. The metastable anatase form of TiO₂, for example, is a more favorable coating of Ti alloys for biomedical applications than the stable rutile form [20,21]. In photocatalysis applications, the presence of both anatase and rutile are desired to realize optimal properties [22,23]. The formation of a particular oxide polymorph on the surface of an oxidized Ti alloy seems to be very dependent on the sequence of suboxides formed during the initial stages of oxidation and methods to select favorable TiO₂ crystal structures during oxidation are actively sought [24–26].

In spite of the apparent complexity of the Ti-O binary there is a remarkable commonality among the stable and metastable Ti oxides and suboxides. Most of the oxides

and suboxides can be viewed as Ti-vacancy and/or oxygen-vacancy orderings over four common parent crystal structures. For example, rutile TiO₂, the Magnéli TiO_{2n-1} phases, and corundum Ti₂O₃ can all be described as different Ti-vacancy orderings over the octahedral interstitial sites of an hcp oxygen sublattice. The anatase TiO₂ and rocksalt TiO phases, in contrast, both share the same fcc oxygen sublattice, differing primarily in the number and arrangement of Ti cations filling octahedral interstitial sites. At Ti rich compositions, oxygen dissolves into hcp Ti, partially filling its octahedral sites. At intermediate temperatures, the dissolved oxygen in hcp Ti is disordered while at low temperature it orders to form the hcp based Ti₆O, Ti₃O, and Ti₂O suboxides. The fourth class of oxides consists of an ω -Ti sublattice with oxygen occupying pyramidally coordinated interstitial sites. Early studies reported a Ti₃O₂ stoichiometry as having an ω -Ti sublattice [27], while the recent study of Amanao *et al.* [6] demonstrated an ability to synthesize TiO having such a crystal structure.

Here we report on a comprehensive first-principles study of phase stability in the Ti-O binary, both at 0 K and at finite temperature. Section III describes a systematic search for the lowest energy oxygen-vacancy and/or titanium-vacancy orderings within four parent crystal structures: (i) hcp Ti, (ii) ω -Ti, (iii) rocksalt TiO, and (iv) hcp oxygen. In Sec. IV we report on a statistical mechanics study of phase stability in the Ti-O system at finite temperature using cluster expansion approaches and Monte Carlo simulations. Section V compares the predicted Ti-O phase diagrams to experimental observations and reveals several discrepancies that are further investigated by exploring the sensitivity of predicted relative stabilities using a range of approximations to DFT and extensions such as DFT +*U* and HSE. We conclude with a discussion of the possible role that vibrational excitations may play in affecting phase stability in the Ti-O system.

*avdv@ucsb.edu

II. METHODOLOGY

First-principles electronic structure methods and statistical mechanics approaches were used to predict phase stability in the Ti-O binary, both at 0 K and at finite temperature. All first-principles calculations were performed with the VASP package [28–31]. The enumeration of different oxygen-vacancy and titanium-vacancy orderings over various parent crystal structures was performed with the CASM software package [32–35]. CASM was also used to construct and parametrize cluster expansion Hamiltonians and to perform finite temperature Monte Carlo simulations.

The majority of first-principles electronic structure calculations were performed within the generalized gradient approximation to density functional theory using the Perdew, Bruke, and Ernzerhof (DFT-PBE) parametrization [36,37]. Benchmark calculations were also performed with other approximations and extensions to DFT. These included the local density approximation (LDA) as parametrized by Perdew and Zunger [38] and other GGA approximations such as those by Perdew and Wang (PW91) [39,40], Perdew, Ruzsinszky, Burke *et al.* revised for solids (PBEsol) [41], and the latest potential developed by Sun, Ruzsinszky, and Perdew (SCAN) [42]. We also used DFT-PBE +*U* following the approach prescribed by Dudarev *et al.* [43] and the hybrid DFT-Hartree Fock approach by Paier *et al.* (HSE) [44] as implemented in VASP.

Interactions between core and valence electrons were accounted for with the projector augmented wave (PAW) pseudopotential method [45,46]. The PAW potentials treat the 3*s*, 3*p*, 3*d*, and 4*s* orbitals of Ti (Ti *sv*) and the 2*s* and 2*p* orbitals of O as valence states. A plane wave energy cutoff of 550 eV was used. A *k*-point convergence analysis was performed for the primitive cells of each distinct parent crystal structure and the *k*-point grids were scaled to ensure the same or higher *k*-point density in reciprocal space for all structures that are supercells of the primitive cells. The following Γ -centered *k*-point grids were found to converge the energy to within 2 meV/atom: (i) a 14 × 14 × 8 *k*-point grid for the suboxides having an hcp Ti sublattice, (ii) a 13 × 8 × 8 *k*-point grid for suboxides and oxides having an ω -Ti sublattice, (iii) a 15 × 15 × 15 *k*-point grid for the rocksalt based oxides, and (iv) a 15 × 15 × 6 *k*-point grid for rutile, which was used to assess *k*-point convergence for the oxides having an hcp O sublattice. All the structures were first relaxed with respect to both their lattice vectors and their internal coordinates to achieve a force convergence of 0.02 eV/Å and an energy convergence of 10⁻⁶ eV. A final static run was performed at the relaxed volume. Partial occupancy during relaxation runs was treated with the method of Methfessel-Paxton (order 2) and the tetrahedron method with Blöchl corrections was used for the static runs.

Most PBE calculations were performed nonspin polarized. Magnetism in titanium oxides is not common and is only expected to occur in the presence of Ti³⁺ ions. This Ti valence may occur in the composition interval between Ti₂O₃ and TiO₂. We performed spin-polarized calculations on all structures residing on the convex hull and found that all ferromagnetically initialized states relaxed to a nonmagnetic state without any local moments. There is some experimental evidence in the literature for the existence of magnetism in the corundum

Ti₂O₃ compound [47,48] and the Magnéli phases [49,50]. These phases all share a common hcp O sublattice with Ti ordering over a subset of octahedral sites. Therefore, all PBE calculations for the structures obtained by decorating the octahedral sites of hcp O with Ti were performed spin polarized. All other benchmark calculations (LDA, PW91, PBEsol, SCAN, HSE, and DFT +*U*) were performed spin polarized.

Cluster expansion Hamiltonians [51–54] were used to parametrize the dependence of the energies of the hcp Ti based suboxides and the rocksalt based oxides as a function of the degree of oxygen-vacancy and titanium-vacancy order. A cluster expansion is a natural parametrization of the energy of a particular parent crystal structure as a function of configurational degrees of freedom. The approach relies on the use of occupation variables σ_i assigned to each oxygen (titanium) sublattice site *i* that is 1 if the site is occupied and 0 if it is vacant (or vice versa depending on the reference configuration). The energy of the crystal can then be expressed as an expansion in terms of polynomials of occupation variables belonging to different sites of a cluster according to [51]

$$E_f\{\vec{\sigma}\} = \sum_{\alpha} V_{\alpha} \phi_{\alpha}, \quad (1)$$

where the cluster functions ϕ_{α} are defined as the product of the site occupation variables belonging to a cluster α ,

$$\phi_{\alpha} = \prod_{i \in \alpha} \sigma_i. \quad (2)$$

The expansion coefficients V_{α} , referred to as effective cluster interactions (ECIs), are to be determined by training on a large set of energies of different oxygen-vacancy and titanium-vacancy orderings. A wide variety of schemes are available to choose the degree of truncation (i.e., which basis functions are included in the expansion) and the numerical values of the ECIs [55–58]. In this work we used a genetic algorithm approach [56] to select the important basis functions and fit the ECIs using a least squares approach picking an expansion that minimizes the cross validation score.

The cluster expansions were implemented in lattice Monte Carlo simulations to calculate finite temperature thermodynamic averages. These were used to generate free energy curves with which temperature versus composition phase diagrams were constructed.

III. GROUND STATE ANALYSIS

We systematically enumerated different Ti-vacancy and/or oxygen-vacancy orderings within four classes of parent crystal structures: (i) hcp Ti with oxygen filling octahedral sites, (ii) rocksalt TiO allowing for Ti-vacancy and oxygen-vacancy orderings over the fcc Ti and fcc O sublattices, (iii) ω -Ti with oxygen filling a subset of the pyramidal interstitial sites, and (iv) hcp O with Ti filling octahedral interstitial sites. More details about the enumerated structures can be found in the Supplemental Material [59].

As measures of concentration, we use *x* to denote the ratio of the number of oxygen N_{O} to the number of titanium N_{Ti} (i.e., $x = N_{\text{O}}/N_{\text{Ti}}$) and *y* to denote the atom fraction [$y = N_{\text{O}}/(N_{\text{Ti}} + N_{\text{O}})$]. To distinguish the different parent crystal

structures, we adopt the following naming scheme. Since hcp Ti is conventionally labeled α , we will refer to any of the suboxides having an hcp Ti sublattice as α -TiO_x. Similarly for the oxides and suboxides that have an ω -Ti sublattice we use ω -TiO_x. The high temperature disordered form of rocksalt is named γ in the literature [1,2]. We will, therefore, refer to rocksalt derived phases using γ and add a prime to distinguish a vacancy ordered rocksalt phase from the disordered solid solution (e.g., γ' -TiO for the ordered phase versus γ -TiO for the disordered phase).

Below we describe the lowest energy orderings in each parent crystal structure. The cell parameters and atomic coordinates of each low energy structure can be found in the Supplemental Material [59]. Formation energies are all expressed relative to the same reference states, taken to be hcp Ti and anatase TiO₂. The formation energies $E_f(y)$ for each suboxide Ti_{1-y}O_y can be expressed as

$$E_f(y) = E(y) - (1 - 3y/2)E[\text{Ti}] - (3y/2)E[\text{TiO}_2], \quad (3)$$

where $E(y)$ is the total energy per atom and $E[\text{Ti}]$ and $E[\text{TiO}_2]$ are the energies per atom of hcp-Ti and anatase TiO₂, respectively.

A. Hcp based TiO_x suboxides

Hcp Ti consists of an ABAB stacking of triangular close-packed planes. Dissolved oxygen in hcp Ti occupies octahedral sites [60]. The collection of octahedral sites between a pair of AB stacked close-packed Ti layers also forms a triangular lattice as illustrated in Fig. 1 and has a C stacking sequence relative to the adjacent Ti AB layers. Every layer of octahedral sites has the same C stacking such that the octahedral sites by themselves form a simple hexagonal lattice within hcp Ti. The number of octahedral interstitial sites is equal to the number of Ti atoms forming the hcp crystal structure. Figure 1 also shows a side view of the hcp crystal with the interstitial octahedral layers labeled as C.

We enumerated 504 different oxygen-vacancy orderings within symmetrically distinct supercells up to a volume of 6 hcp primitive unit cells. Figure 2(a) shows the calculated formation energies of these orderings. Also shown in Fig. 2(a) is the global convex hull, connecting the lowest energy orderings over all four families of parent crystal structures considered in this work.

There are three ground state orderings when considering only the oxygen-vacancy configurations in hcp TiO_x: α -Ti₆O, α -Ti₃O, and α -Ti₂O. The first ground state α -Ti₆O has oxygen filling one out of every six octahedral sites. They segregate to every other layer along the c axis resulting in a staged ordering. The filled layers have an oxygen composition of 1/3 with oxygen ordering on a $\sqrt{3}a \times \sqrt{3}a$ two-dimensional supercell of the triangular lattice. This ordering is shown in Fig. 3(a). The second ground state α -Ti₃O is very similar to α -Ti₆O in that it is also staged along the c axis and has oxygen ordered on a $\sqrt{3}a \times \sqrt{3}a$ supercell within the filled layers. The filled layers, however, now have a composition of 2/3 as illustrated in Fig. 3(b). The two-dimensional supercells of each filled layer in Ti₆O and Ti₃O are staggered relative to each other along the c axis. Both the Ti₆O and Ti₃O low energy orderings are

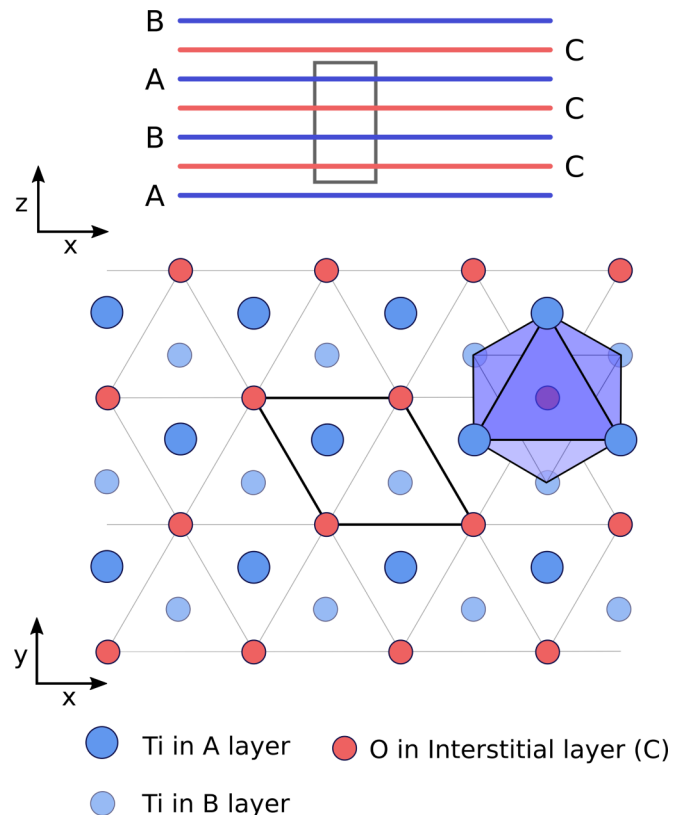


FIG. 1. Depiction of the hcp crystal structure represented as an AB stacking of close packed triangular lattices of metal atoms. Interstitial oxygen fills octahedral voids formed by the metal atoms in the interstitial layers. These sites also form a two-dimensional triangular lattice that has a C stacking relative to the hcp crystal.

consistent with those predicted to be ground states in previous first-principles studies [61,62]. The third predicted ground state with the α -Ti₂O stoichiometry has 1/2 of its octahedral sites filled by oxygen. This ordering is not staged but has oxygen instead filling each layer uniformly. Within each layer, the oxygens arrange in a zigzag pattern separated by zigzags of vacant sites as illustrated in Fig. 3(c). The zigzag rows are staggered when going from one interstitial layer to the next avoiding oxygen overlap between adjacent layers along the c axis. This ordering was also found to be a ground state by Burton and van de Walle [61].

B. Rocksalt based oxides

The rocksalt crystal structure consists of two fcc sublattices with the sites of one fcc sublattice filling the octahedral sites of the other fcc sublattice. Titanium and oxygen can form a rocksalt based crystal structure in which Ti occupies one fcc sublattice and oxygen the other. A rocksalt type phase is observed at high temperatures, which is reported to be stable in a wide concentration range ($0.45 < y < 0.6$ for Ti_{1-y}O_y). This phase is usually referred in the literature as γ -TiO and contains vacancies on both the Ti and O sublattices that are disordered at high temperature [63].

Remarkably, the low temperature, stoichiometric form of equiatomic TiO contains an equal number of oxygen and

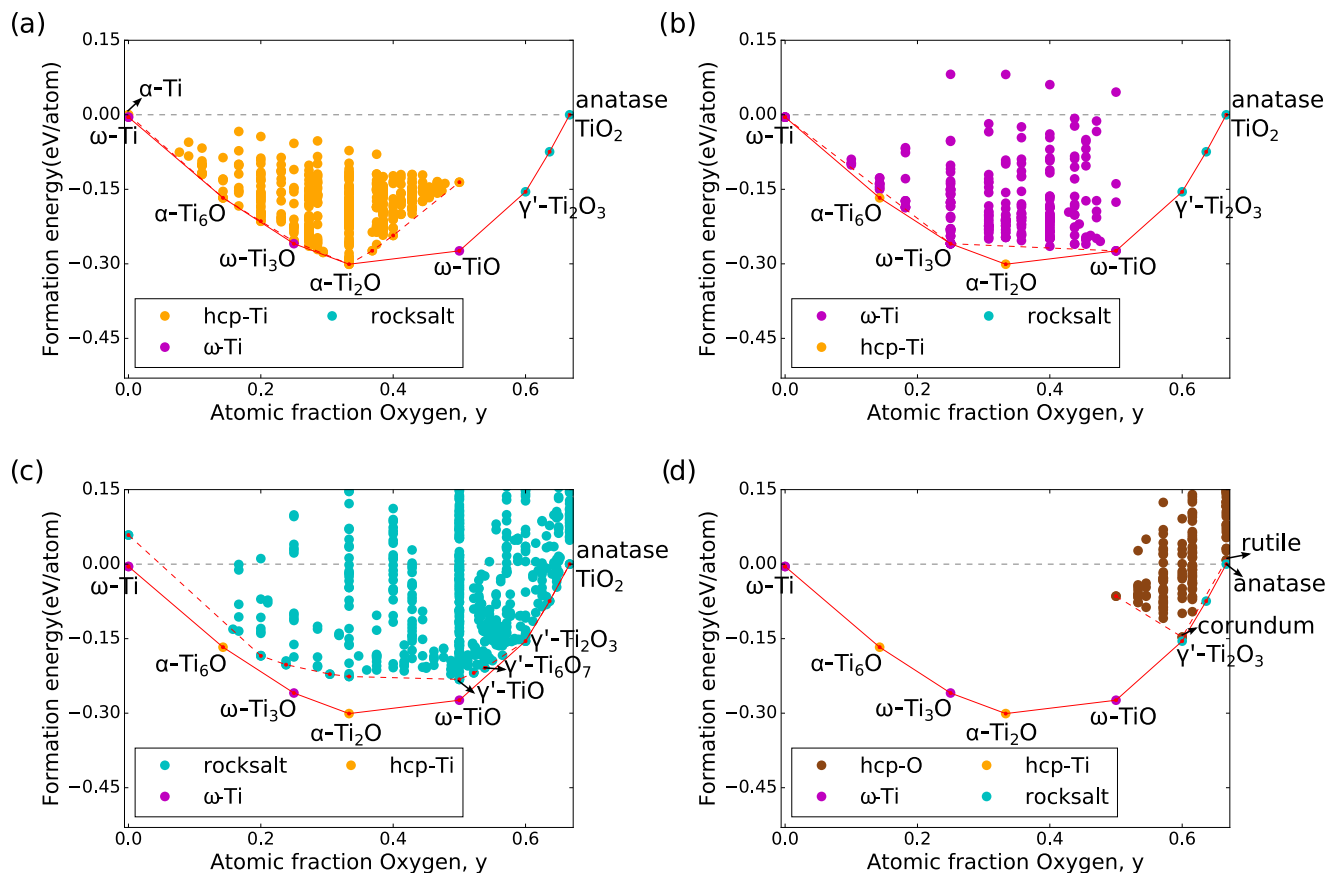


FIG. 2. Formation energies of enumerated oxygen-vacancy and/or titanium-vacancy orderings within (a) hcp Ti (labeled α), (b) ω -Ti, (c) rocksalt, and (d) hcp oxygen. The global convex is shown as solid lines and the metastable convex hulls of each parent crystal structure are shown using dashes lines. The formation energies are calculated relative to hcp Ti and anatase TiO_2 .

titanium vacancies on each fcc sublattice that order to form a supercell containing six primitive rocksalt TiO unit cells [64]. In this ordering, one out of every six Ti and O sublattice sites are vacant. The unit cell and vacancy ordering is illustrated in Fig. 4. In the literature, this ordered rocksalt has been

referred to as α - TiO , Ti_5O_5 , or monoclinic- TiO [1,65]. To avoid confusion with hcp Ti and its suboxides, which are also referred to as α , we will label the low temperature ordered rocksalt as γ' - TiO , where γ indicates that it is derived from rocksalt and the prime signifies that it is ordered.

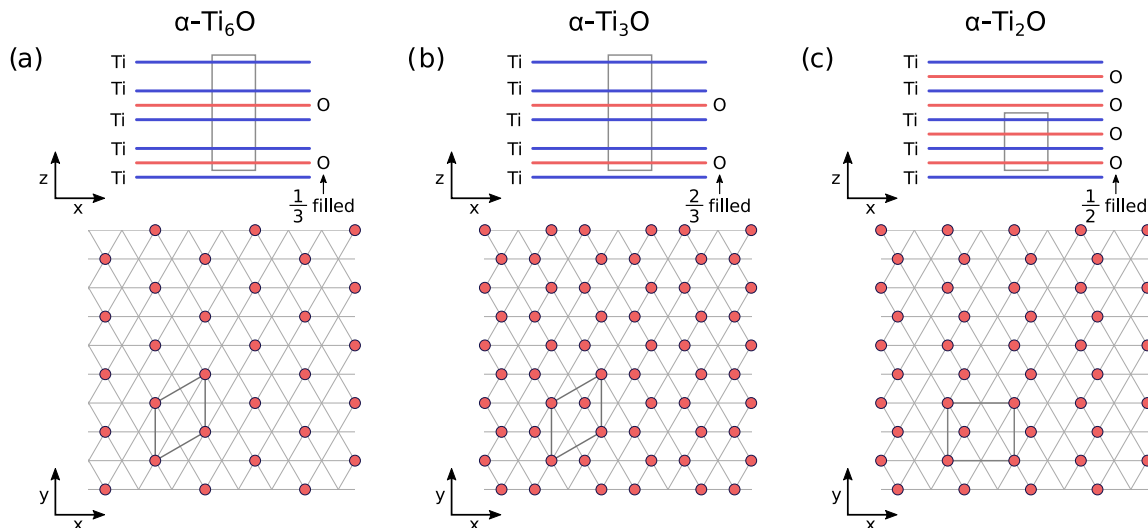


FIG. 3. Ground state oxygen orderings over the interstitial sites of hcp Ti: (a) α - Ti_6O , (b) α - Ti_3O , and (c) α - Ti_2O . In α - Ti_6O and α - Ti_3O the oxygen fills alternating layers and forms a $\sqrt{3}a \times \sqrt{3}a$ supercell parallel to the hcp basal plane. The oxygen of α - Ti_2O order as zigzag rows.

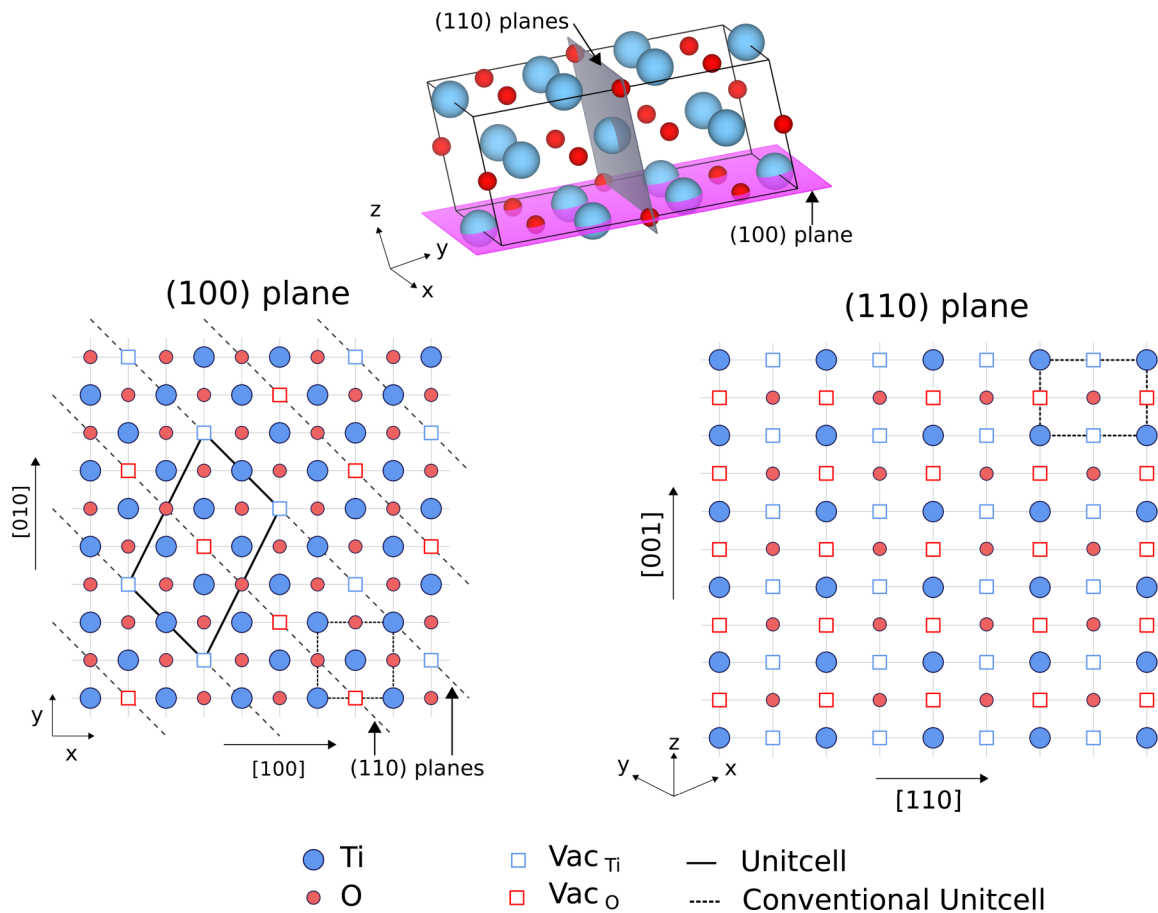


FIG. 4. Illustration of the γ' -TiO structure. Titanium and oxygen vacancies coalesce on every third (110) plane of the conventional rocksalt unit cell.

The anatase form of TiO_2 is also related to rocksalt in that it consists of an fcc oxygen sublattice with Ti ordered over half the octahedral interstitial sites. It can be derived from perfect rocksalt TiO by replacing half the Ti with vacancies. In fact, it is well known that having a precursor rocksalt phase fosters the further formation of anatase as opposed to rutile during the oxidation of Ti alloys [26].

To explore phase stability in the rocksalt parent crystal structure as a function of concentration, we systematically enumerated 720 vacancy orderings over the Ti and O sublattices of rocksalt TiO in supercells that contain up to 12 rocksalt primitive cells. Figure 2(c) shows the calculated formation energies for all the rocksalt derived orderings. Also shown is the global convex hull over the four parent crystal structures. There are five orderings at oxygen rich concentrations that reside on the convex hull. These include anatase TiO_2 at a mole fraction of $y = 2/3$ and the experimentally observed vacancy ordered γ' -TiO (mole fraction $y = 1/2$). Three additional ground states are predicted that we label γ' - Ti_6O_7 (mole fraction $y = 0.538$), γ' - Ti_2O_3 (mole fraction $y = 0.6$), and γ' - Ti_4O_7 (mole fraction $y = 0.636$), with the prime again signifying that they are vacancy ordered rocksalt phases. The γ' - Ti_4O_7 ordering barely breaks the convex hull and is nearly degenerate in energy with a two-phase mixture of γ' - Ti_2O_3 and anatase- TiO_2 .

The three ground state orderings γ' -TiO, γ' - Ti_6O_7 , and γ' - Ti_2O_3 exhibit very similar vacancy arrangements. Figure 4

illustrates the vacancy ordering within γ' -TiO. Both the oxygen and titanium vacancies coalesce on one out of every three parallel (110) planes of the parent rocksalt crystal. Within those planes they order into a checker boardlike pattern also shown in Fig. 4. The γ' - Ti_2O_3 ground state only has Ti vacancies and these again coalesce on one out of every three parallel (110) planes of rocksalt as illustrated in Fig. 5(a).

The vacancy ordering in γ' - Ti_6O_7 is slightly more complex than in the two other ground states since the vacancies coalesce to every (110) plane. Within each (110) plane, however, there are strips with a Ti- and O-vacancy arrangement as in TiO and strips that contain no vacancies. This ordering within the (110) planes is illustrated in Fig. 5(b). The (110) planes are then staggered in the three-dimensional crystal such that a strip containing vacancies neighbors strips that do not contain vacancies in the adjacent (110) planes.

C. ω -Ti based suboxides

Experimental studies have identified suboxides with an ω -Ti sublattice. The ω -Ti crystal structure is in fact the stable form of Ti at low temperatures and is predicted by PBE to have a lower energy than hcp Ti [66,67]. The ω -Ti sublattice consists of two-dimensional honeycomb planes, labeled H, interleaved by triangular layers, labeled T (Fig. 6). The unit cell has three Ti atoms. The Ti atoms of the triangular layers stack directly above and below the empty hexagonal rings of the honeycomb

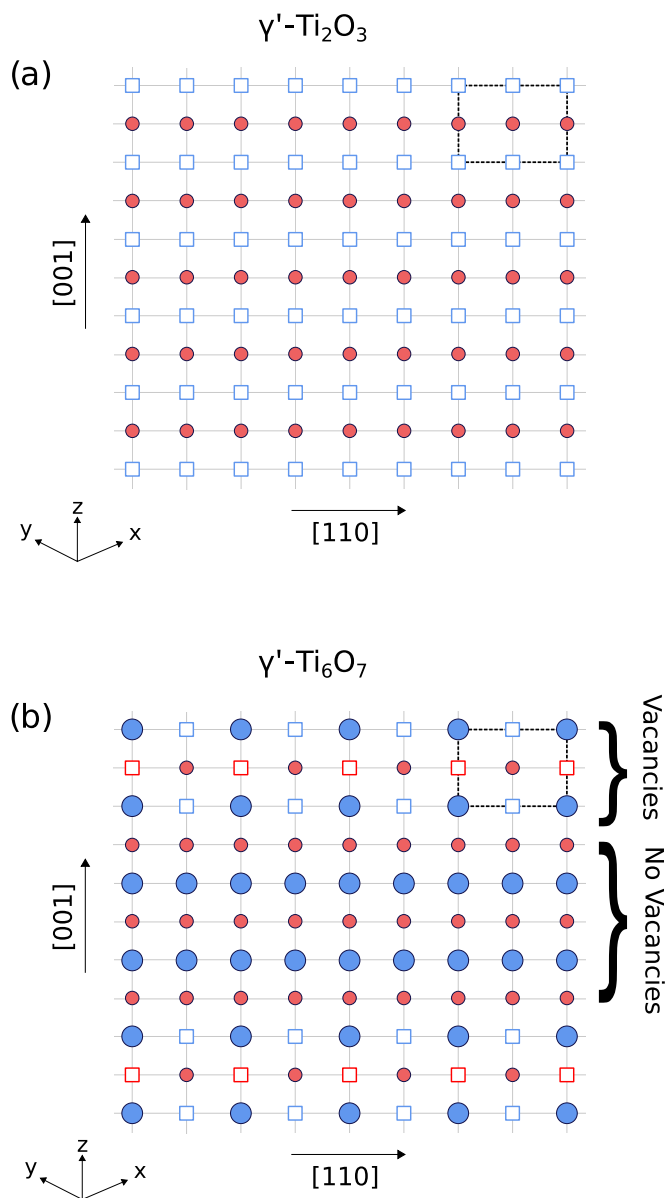


FIG. 5. Vacancy orderings over the titanium and oxygen sites of a (110) plane of rocksalt for (a) γ' - Ti_2O_3 and (b) γ' - Ti_6O_7 .

planes as illustrated in Fig. 6. The ω -Ti sublattice has a variety of large interstitial sites all centered within the triangular T layers that can be occupied by oxygen. One set of interstitial sites are coordinated by Ti forming a square pyramid. These are shown in Fig. 6(b). There are two such sites for every Ti, however, pairs of pyramidal sites share faces, thereby, making it energetically very unfavorable to simultaneously occupy neighboring sites. Oxygen can also occupy the center of the square base between pairs of pyramidal sites. These are shown in Fig. 6(c). There are a total of two square pyramidal sites and one square base site per Ti in the ω crystal structure.

We enumerated over 293 oxygen-vacancy configurations in ω -Ti with oxygen either in the square pyramidal sites or at the center of their base. Due to their close proximity, we never allowed simultaneous occupation of nearest neighbor pyramidal sites. Figure 2(b) shows the formation energies

of the different configurations along with the global convex hull over all structures considered in this work. As is clear in Fig. 2(b), two orderings having the ω -Ti sublattice reside on the global convex hull. The first is the ω - Ti_3O and has an atom fraction $y = 0.25$, while the second has atom fraction $y = 0.5$ corresponds to ω -TiO. There is, however, no ω -Ti based ground state having a stoichiometry of Ti_3O_2 as reported in early experimental studies [27,60,68].

In the ω -TiO ground state, the oxygen occupies half the Ti-square pyramidal sites. As is clear in Fig. 7(a), the oxygen in the ω -TiO ground state fill alternating pyramidal sites. There are two symmetrically equivalent variants of this ordering. One variant can be transformed into the other by passing each oxygen through the square base of its pyramidal site to its neighboring square pyramidal site. Figure 8 shows how the energy of the crystal varies along this path. In the ω -TiO ground state, the square base site, corresponding to the midpoint along this path, is an unstable position and coincides with a local maximum in the energy surface of Fig. 8. Furthermore, the barrier to uniformly go from one ground state variant to the other is very large. The ground state ω -based TiO configuration is predicted to be more stable than the rocksalt γ' -TiO configuration. In fact the phase was recently synthesized by Amano *et al.* [6]. While they labeled it the ϵ phase, we will refer to it as ω -TiO to emphasize its relation to the ω crystal structure.

The other ω -Ti based ground state at lower oxygen fraction ω - Ti_3O has oxygen occupying one third of the square base sites. Its ordering is shown in Fig. 7(b). Inspection of the relaxed oxygen-vacancy configurations within ω - TiO_x revealed a shift in the preference for the square pyramidal sites to the square base of the pyramidal sites as the oxygen concentration decreases. Figure 8 shows that the square base sites of ω - Ti_3O are a shallow minimum as a function of oxygen displacements that take it from the square base sites to the centers of the adjacent pyramidal sites.

D. Hcp oxygen based oxides

A large number of the oxygen rich oxides of Ti can be mapped onto structures having an hcp oxygen sublattice with different Ti-vacancy orderings over the interstitial octahedral sites of the oxygen sublattice. We enumerated 177 different Ti-vacancy configurations over the octahedral sites of hcp oxygen within supercells up to four times the primitive hcp cell. The calculated formation energies are shown in Fig. 2(d). While all calculations were performed with spin polarization, only a fraction of the configurations maintained a finite (ferromagnetic) moment after relaxation. The corundum Ti_2O_3 and rutile TiO_2 structures, for example, relaxed to nonmagnetic states. Two Magnéli phases, though, remained ferromagnetic (Ti_4O_7 and Ti_5O_9). Surprisingly none of the hcp oxygen based orderings reside on the global convex hull. While it is well known that most approximations to DFT predict that anatase is more stable than rutile TiO_2 [69–74], Fig. 2(d) shows that the corundum form of Ti_2O_3 is also predicted to be less stable than the predicted rocksalt based ground state γ' - Ti_2O_3 . Furthermore, none of the Magnéli based phases, which are derived from rutile, reside on the global convex hull.

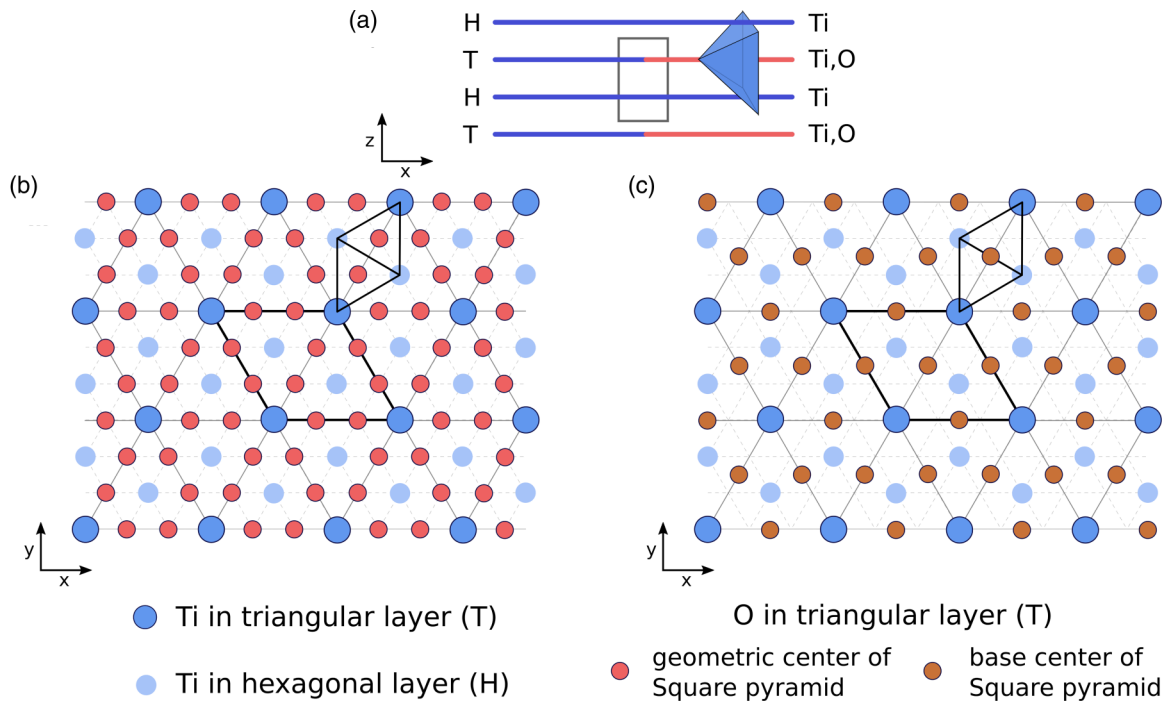


FIG. 6. Illustration of the ω -Ti crystal and candidate interstitial sites. The ω crystal structure is made up of honeycomb (H) layers alternated by triangular layers (T) as shown in (a) and has square pyramidal interstitial sites that can be occupied by oxygen. Oxygen can also reside at the base center of a square pyramidal site. (b) and (c) The arrangement of Ti and O atoms in the T and H layers, respectively.

IV. FINITE TEMPERATURE PHASE STABILITY

Experiments suggest that hcp and rocksalt based suboxides form solid solutions that are stable over large composition ranges at high temperature [1,2]. In hcp, the ordered suboxides undergo order-disorder transitions upon heating in which oxygen and vacancies disorder to form a high temperature solid solution [75]. The oxygen and titanium vacancies of the rocksalt based phases, which are ordered at low temperature, can also disorder to form a high temperature solid solution [76].

We investigated these order-disorder transitions and the high temperature disordered solid solutions by combining DFT-PBE parametrized cluster expansions with Monte Carlo simulations. For hcp based TiO_x we constructed a cluster expansion that describes the configurational energy for oxygen-vacancy disorder over the octahedral sites of the hcp Ti sublattice. The parameters of the expansion were fit to 350 DFT-PBE formation energies using a genetic algorithm to determine an optimal set of interaction coefficients. The cluster expansion fit has the weighted cv score of 3.2 meV/unit cell and a weighted rms of 2.9 meV/unit cell. The weights on the configurations reduce exponentially with increasing distance from the convex hull.

We also constructed a cluster expansion to describe the configurational energy of vacancies over both the Ti and O sublattices of rocksalt TiO. This cluster expansion is capable of describing the vacancy ordered γ' -TiO rocksalt phase as well as the other ground states that can be derived from rocksalt by introducing vacancies on the Ti and O sublattices. These include the ground states having Ti_6O_7 and Ti_2O_3 stoichiometries and anatase TiO_2 . The cluster expansion does not predict the marginally stable Ti_4O_7 ground state as residing on the

convex hull. A total of 611 DFT-PBE formation energies were used to parametrize the interaction coefficients of the rocksalt cluster expansion. The cluster expansion fit has a cv score of 34 meV/unit cell and the weighted rms of 25 meV/unit cell with weights scaled towards compounds in the composition region of interest.

Grand canonical Monte Carlo simulations were performed on the two cluster expansions to calculate thermodynamic averages, including average concentrations, grand canonical energy, heat capacity, and the covariances of the number of oxygen/vacancies within the crystal, all as a function of temperature and oxygen chemical potential. The thermodynamic averages were then used to generate free energies with conventional free energy integration techniques [8,77–79]. Application of the common tangent construction to the Gibbs free energies then enabled the construction of finite temperature phase diagrams.

Figure 9(a) shows a calculated temperature versus composition phase diagram for hcp based TiO_x and rocksalt $\text{Ti}_{(1-y)}\text{O}_y$. The phase diagram does not include the ω -Ti based suboxides, which are on the global convex hull at 0 K but were left out when applying the common tangent construction to calculated Gibbs free energies. This was done to facilitate comparison to experimental assessments which do not yet include the ω -Ti based oxide phases [1,2]. Furthermore, none of the oxides having an hcp oxygen sublattice (i.e., rutile, Magnéli, and corundum) appear in the calculated phase diagram since they are not predicted as global ground states. Hence the phase diagram of Fig. 9(a) is a metastable phase diagram and represents phase stability under the assumption that the ω -Ti based suboxides are prevented from forming due, for example, to kinetic factors.

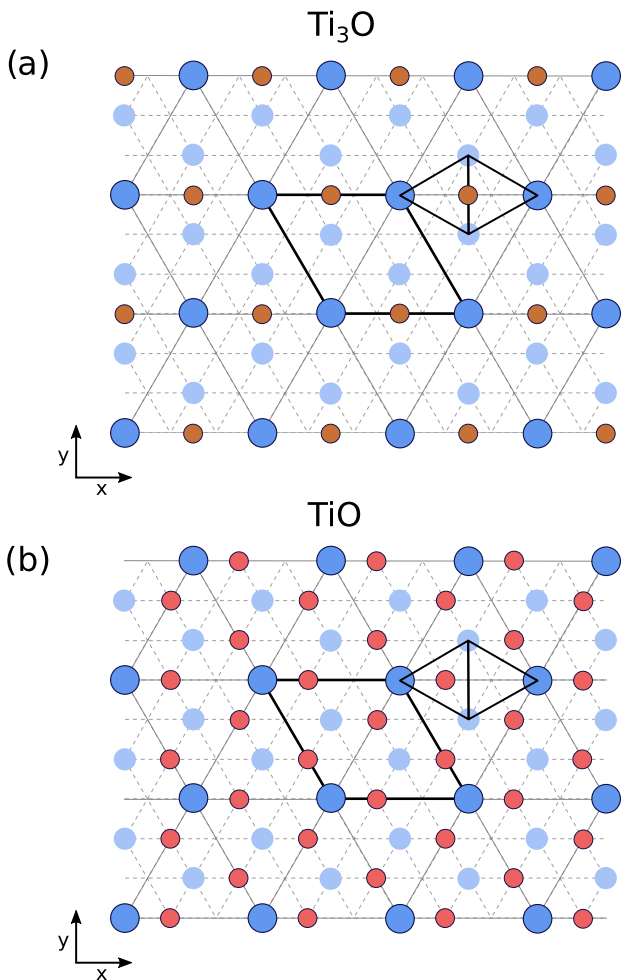


FIG. 7. Oxygen orderings within the T layers of (a) ω -Ti₃O and (b) ω -TiO.

The metastable phase diagram of Fig. 9(a) shows that the hcp Ti based suboxides, α -Ti₆O, α -Ti₃O, and α -Ti₂O, disorder to form a solid solution at intermediate temperatures, with stoichiometric Ti₆O and Ti₂O having order-disorder transition temperatures of approximately 1000 K. The solid solution, however, is stable to lower temperatures at compositions away from the ideal ordering stoichiometries. The α -Ti₆O suboxide phase is also predicted to be stable over a wide oxygen concentration range. The excess oxygen is accommodated in the vacant sites of the filled oxygen layers of the α -Ti₆O ordering [Fig. 3(a)] without disrupting the $\sqrt{3}a \times \sqrt{3}a$ superlattice periodicity. Inspection of the heat capacity and the covariance of the oxygen concentration as a function of temperature and chemical potential suggests the existence of a second order transition between α -Ti₃O and oxygen excess α -Ti₆O. This is represented by the dashed line in Fig. 9(a). The high temperature hcp based solid solution is predicted to be stable up to an oxygen concentration of $y \approx 0.33$ before it decomposes into a rocksalt based oxide.

The calculated phase diagram of Fig. 9(a) replicates the vast solid solution region of hcp TiO_x at higher temperatures as observed experimentally and provides more clarity about phase stability at low temperature. It is also consistent with

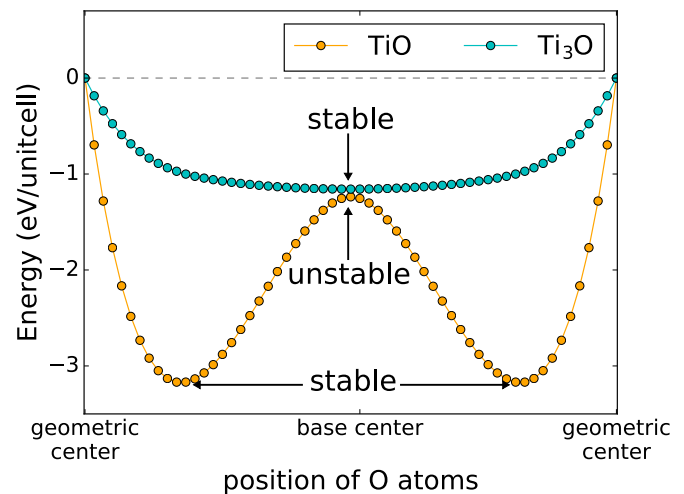


FIG. 8. Energy landscape along the path joining pyramidal and base center interstitial positions in the ground state structures of ω -Ti₃O and ω -TiO.

a previous first-principles study of the hcp TiO_x portion of the phase diagram by Burton and van de Walle [61], although there is a difference in the predicted order-disorder transition

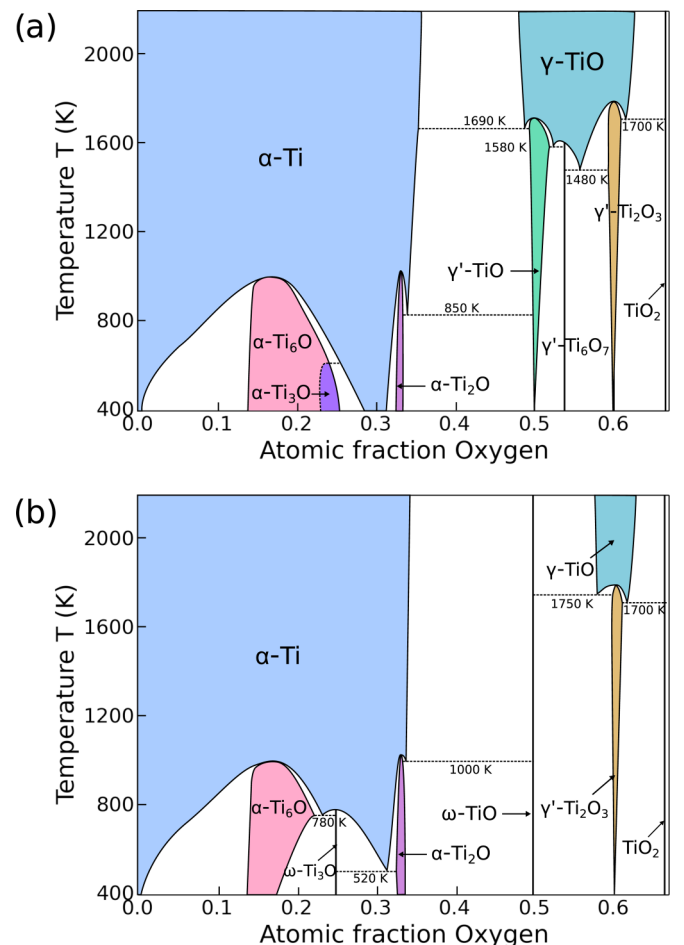


FIG. 9. Calculated binary metastable and equilibrium Ti-O phase diagrams. (a) Metastable phase diagram calculated by excluding the ω -Ti based parent crystal structure. (b) Equilibrium phase diagram calculated by considering all four parent crystal structures.

temperature of Ti_2O . The present study also predicts a second order transformation between the $\alpha\text{-Ti}_6\text{O}$ and $\alpha\text{-Ti}_3\text{O}$, while such a transition is not predicted in the previous study. These disparities are likely due to differences in the parametrization of the cluster expansion Hamiltonian. The cluster expansion of the present study was parametrized with three times as many DFT calculations as were used in the earlier studies.

Figure 9(a) shows that the rocksalt orderings are predicted to disorder at temperatures between 1600 and 1700 K. This is substantially higher than the transition temperatures reported in assessed phase diagrams based on experimental measurements [80]. The disordered rocksalt phase is stable in a wide concentration range at high temperature, consistent with assessed phase diagrams of the Ti-O binary [1,2].

Figure 9(b) shows a calculated phase diagram when all four parent crystal structures are considered and represents global phase stability as predicted with DFT-PBE. In constructing the phase diagram of Fig. 9(b) all $\omega\text{-Ti}$ based suboxides were treated as line compounds. Configurational entropy favors hcp TiO_x at high temperature with $\omega\text{-Ti}_3\text{O}$ (treated as a line compound) transforming to an hcp TiO_x solid solution at approximately 800 K. Figure 9(b) also shows that configurational entropy within the rocksalt host is not large enough to overcome the energy difference between $\omega\text{-TiO}$ and $\gamma'\text{-TiO}$ predicted at 0 K with DFT-PBE, with $\omega\text{-TiO}$ predicted to be stable at all temperatures considered. The high temperature disordered $\gamma\text{-TiO}$ rocksalt is still predicted to form, but only at concentrations where the oxygen content is higher than the Ti content.

V. DISCUSSION

The Ti-O binary has a remarkably rich variety of stable and metastable oxides and suboxides. Our systematic investigation of phase stability over four parent crystal structures (i.e., $\alpha\text{-TiO}_x$, $\omega\text{-TiO}_x$, rocksalt derived oxides, and oxides having an hcp oxygen sublattice) has shown that DFT is capable of accurately describing important features of the Ti-O binary phase diagram. The combination of DFT-PBE calculations and cluster expansion approaches to account for configurational degrees of freedom predict an oxygen solubility in hcp Ti of approximately 0.33%, in excellent agreement with experiment. Furthermore, the oxygen within hcp Ti is predicted to order at low temperature as observed experimentally [81–83]. DFT-PBE also predicts that the experimentally observed vacancy ordered rocksalt $\gamma'\text{-TiO}$ is a ground state when considering all vacancy orderings over the Ti and O sublattices of rocksalt. Monte Carlo simulations show that the vacancy ordered rocksalt phases undergo order-disorder transitions to form a high temperature disordered rocksalt solid solution over an extended oxygen composition. This is again qualitatively consistent with experimental observations and assessed phase diagrams, although the predicted order-disorder transition temperatures are substantially higher than reported ones [80].

Notwithstanding the many qualitative similarities between the calculated and experimentally assessed phase diagrams, there are also subtle but important differences. For example, it has already been well-established that most approximations to DFT predict the anatase form of TiO_2 as having a lower energy than rutile [69–74], while common interpretations of

experiment indicate that the reverse should be true [84,85]. The results of the present study suggest that additional discrepancies occur at lower Ti/O ratios. The corundum crystal structure of Ti_2O_3 has been reported in many experimental studies [48,60]. Nevertheless, DFT-PBE predicts a vacancy ordering in rocksalt as the ground state at the Ti_2O_3 stoichiometry. We are unaware of any experimental reports of a rocksalt derived ordering having the same composition. At the TiO stoichiometry, the $\omega\text{-TiO}$ phase is predicted to be the ground state, while assessed phase diagrams include the rocksalt form of $\gamma'\text{-TiO}$ as the equilibrium phase at low temperature (usually labeled $\alpha\text{-TiO}$) [1,2]. The vacancy ordered rocksalt form of $\gamma'\text{-TiO}$ has been well characterized experimentally and studied theoretically [60,64,86,87]. It is only recently that an $\omega\text{-TiO}$ phase has been successfully synthesized using indirect routes [6]. Early reports by Andersson [27] of the existence of Ti_3O_2 having an $\omega\text{-Ti}$ sublattice confuse matters further. The PBE convex hull of Fig. 2(b) does not exhibit a ground state having a stoichiometry of Ti_3O_2 , with the formation energies of $\omega\text{-Ti}$ based orderings being well above the hull at this composition. Andersson, however, was not able to isolate the purported Ti_3O_2 line compound but rather studied multiphase mixtures that may well have included an $\omega\text{-TiO}$ instead.

Discrepancies between DFT predicted ground states and experiment also exist for the suboxides. The diffraction patterns for the three ordered suboxides having an hcp Ti sublattice suggest stage ordering with oxygen filling alternating layers between close-packed Ti layers [82]. This is consistent with the ground state predictions for $\alpha\text{-Ti}_6\text{O}$ and $\alpha\text{-Ti}_3\text{O}$, but the predicted ground state for $\alpha\text{-Ti}_2\text{O}$ is not staged. The oxygen ordering of $\alpha\text{-Ti}_2\text{O}$ consists of zigzag oxygen rows separated by equivalent rows of vacancies within each oxygen layer [Fig. 3(c)] and is predicted to have an energy that is 22 meV/atom lower than the stage-ordered form of Ti_2O . Another apparent inconsistency among the suboxides is the prediction that $\omega\text{-Ti}_3\text{O}$ is a global ground state and is stable up to approximately 800 K. There is, though, no experimental evidence for the existence of an $\omega\text{-Ti}_3\text{O}$ suboxide.

While our study accounted for configurational degrees of freedom, vibrational excitations are also likely to be important at elevated temperature. The inclusion of vibrational degrees of freedom could qualitatively modify several of the predicted 0 K relative stabilities. In fact, recent experimental and first-principles studies of TiO_2 have demonstrated the importance of anharmonicity in rutile and have pointed to the possibility that vibrational excitations could reverse the relative stability between rutile and anatase at intermediate and high temperatures [88,89]. Vibrational excitations are also likely important at low oxygen concentrations. The $\omega\text{-Ti}$ phase is the ground state in the absence of oxygen, but transforms to hcp $\alpha\text{-Ti}$ at intermediate temperatures due to a difference in vibrational entropy [90]. A similar difference in vibrational entropy may reverse the predicted relative stability between $\alpha\text{-Ti}_3\text{O}$ and $\omega\text{-Ti}_3\text{O}$ at intermediate temperatures considering that these two crystals differ in energy by only 4 meV/atom. Vibrational excitations may also affect the relative stability between $\omega\text{-TiO}$ and $\gamma'\text{-TiO}$. An investigation of phase stability in the chemically similar Zr-O binary showed that the ZrO monoxide having the same crystal structure as $\omega\text{-TiO}$ [34,91] has less vibrational entropy than the other oxides in the Zr-O

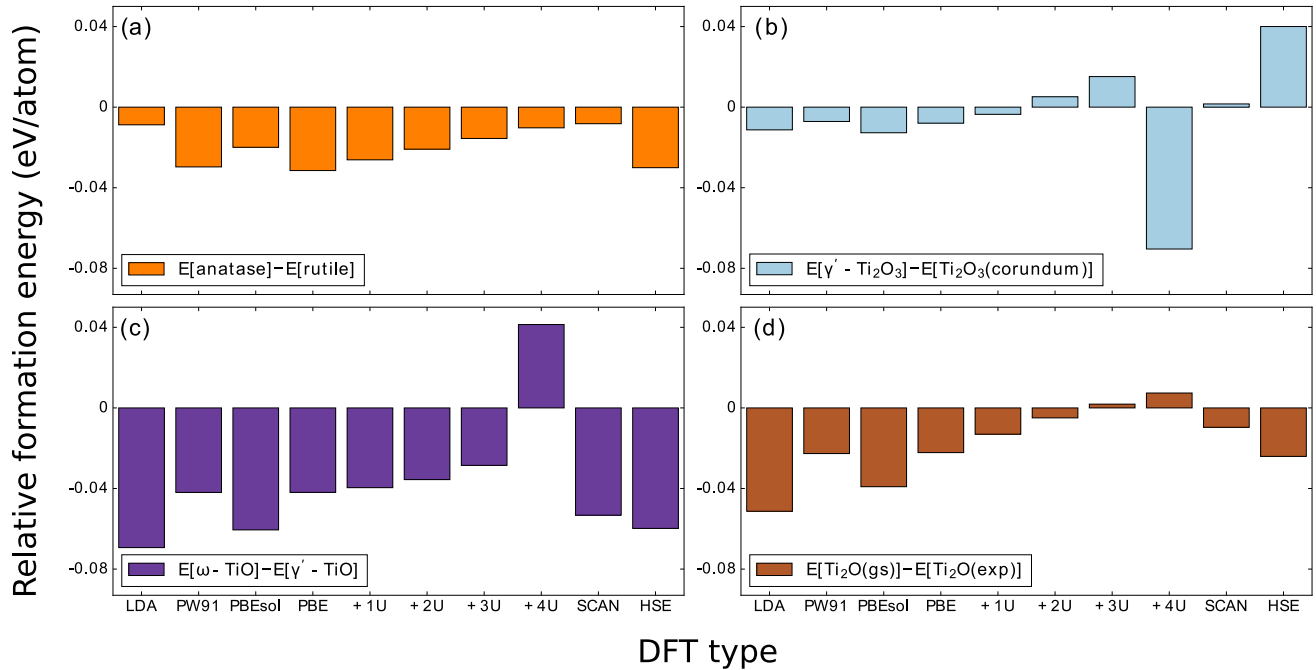


FIG. 10. Dependence of the relative stability between competing polymorphs on the various approximations to density functional theory. (a) The energy difference between anatase and rutile TiO_2 (negative values signify anatase as a lower energy and stable polymorph), (b) energy difference between rocksalt γ' - Ti_2O_3 and corundum Ti_2O_3 , (c) energy difference between ω - TiO and γ' - TiO , and (d) energy difference between the ground state (gs) zigzag ordered α - Ti_2O and experimental (exp) staged Ti_2O .

system [92]. The importance of anharmonic vibrational excitations in the oxides of the Ti-O system [88,89] complicates the treatment of vibrational contributions to the free energy as it requires models that go beyond the quasiharmonic approximation [33,93–95].

The discrepancies between predicted ground states and experiment may also be due to a failure of DFT-PBE. The relative stability between anatase and rutile TiO_2 has been studied extensively in the past using a wide variety of approximations to DFT and its extensions. This includes LDA, PBE, PW91, DFT + U , HSE, and the random phase approximation (RPA) [69–74,96]. It is only with DFT + U employing values of U in excess of 6 eV or with the random phase approximation that the relative stability between anatase and rutile is reversed [96]. Figure 10 shows the sensitivity of the difference in energy between the competing polymorphs at the TiO_2 , Ti_2O_3 , TiO , and Ti_2O stoichiometries as calculated with different approximations to DFT (i.e., LDA, PW91, PBE, PBEsol, and the recently developed SCAN potential) and the extensions to DFT with + U and hybrid functional methods (HSE). All calculations in Fig. 10 were performed spin polarized [97].

Figure 10 shows that almost all approximations are qualitatively consistent with DFT-PBE, including the newly developed SCAN exchange-correlation functional. The results of Fig. 10(a) are consistent with past studies [69–74], showing that most approximations to DFT predict anatase as more stable than rutile. Even the newly developed SCAN exchange correlation functional predicts anatase as the ground state. Predictions with HSE are also consistent with PBE for Ti_2O , TiO , and TiO_2 . Only in the case of Ti_2O_3 does HSE reverse the PBE predicted relative stability between corundum and the vacancy ordered rocksalt phase. SCAN predicts that corundum

and the low energy vacancy ordered rocksalt are essentially degenerate within the numerical error of the VASP calculations, the difference between the two polymorphs of Ti_2O_3 being less than 1 meV/atom with SCAN. Figures 10(c) and 10(d) show that large values of U (above 3–4 eV) within the DFT + U approximation will reverse the relative stability between γ' - TiO and ω - TiO and between the staged and zigzag row ordered α - Ti_2O . It is, however, questionable whether DFT + U is an accurate description at these Ti rich concentrations, especially for Ti_2O .

The strong affinity between titanium and oxygen and the difficulty of eliminating other impurities such as hydrogen, carbon, and nitrogen that also react to form compounds with titanium make this system especially challenging to study experimentally. Interstitial impurities such as carbon and nitrogen favor a rocksalt compound with Ti [98,99] and if present as contaminants can play a role in selecting out the rocksalt form of TiO [24], which DFT calculations predict as being metastable relative to the ω - TiO . Intrinsic kinetic barriers between the hcp Ti sublattice of α - TiO_x and the ω -Ti sublattice of ω - Ti_3O and ω - TiO [100] may also play a role in suppressing the formation of what DFT predicts are equilibrium phases.

VI. CONCLUSION

We have performed a comprehensive first-principles study of phase stability in the Ti-O binary both at 0 K and at finite temperature by accounting for configurational degrees of freedom. Many qualitative features of the predicted equilibrium and metastable phase diagrams agree with experimental observations. This includes a prediction of an exceptionally

high oxygen solubility in hcp Ti, the stability of oxygen ordering within hcp Ti at low temperature, and the stability of rocksalt based oxides having high concentrations of both oxygen and titanium vacancies at intermediate concentrations. Our study also reveals important discrepancies between predicted ground state structures and experimentally observed phases. The inclusion of vibrational contributions to the free energy may rectify several of these discrepancies and should be the focus of future studies. It is also possible that more advanced electronic structure methods that go beyond DFT and its common extensions may be required to accurately describe the physics of several of the oxides in the Ti-O binary. Many of the assessed Ti-O phase diagrams [1,2] rely on experimental studies that were performed almost a half century ago. Experimental studies are suggested to further refine the crystal structures of the oxides and suboxides in this complex system. The results of this study suggest a different ordering for

α -Ti₂O than was inferred from past diffraction studies [82] and the possibility of additional vacancy ordered rocksalt phases.

ACKNOWLEDGMENTS

We acknowledge our funding source, NSF DMREF Grant DMR1436154 DMREF: Integrated Computational Framework for Designing Dynamically Controlled Alloy-Oxide Heterostructures. The computations were performed using resources supported by the Center for Scientific Computing, CNSI and MRL under NSF MRSEC (DMR-1720256). Computing resources were also provided by National Energy Research Scientific Computing Center, a DOE Office of Science User Facility supported by the Office of Science of the US Department of Energy under Contract No. DE-AC02-05CH11231. The plots were made using the matplotlib python library [101].

-
- [1] J. L. Murray and H. A. Wriedt, *J. Phase Equilib.* **8**, 148 (1987).
 [2] H. Okamoto, *J. Phase Equilib. Diffusion* **32**, 473 (2011).
 [3] H. A. Wriedt and J. L. Murray, *Binary Alloy Phase Diagrams*, edited by T. B. Massalski (American Society for Metals, Metals Park, OH, 1986), p. 1655.
 [4] H. Okamoto, *J. Phase Equilib. Diffusion* **27**, 306 (2006).
 [5] J. L. Murray, P. K. Liao, and K. E. Spear, *Bull. Alloy Phase Diagrams* **7**, 550 (1986).
 [6] S. Amano, D. Bogdanovski, H. Yamane, M. Terauchi, and R. Dronskowski, *Angew. Chem., Int. Ed.* **55**, 1652 (2016).
 [7] J. Bhattacharya and A. Van der Ven, *Phys. Rev. B* **81**, 104304 (2010).
 [8] A. S. Dalton, A. A. Belak, and A. Van der Ven, *Chem. Mater.* **24**, 1568 (2012).
 [9] A. A. Belak, Y. Wang, and A. Van der Ven, *Chem. Mater.* **24**, 2894 (2012).
 [10] M. Wagemaker, W. J. H. Borghols, and F. M. Mulder, *J. Am. Chem. Soc.* **129**, 4323 (2007).
 [11] W. J. H. Borghols, M. Wagemaker, U. Lafont, E. M. Kelder, and F. M. Mulder, *J. Am. Chem. Soc.* **131**, 17786 (2009).
 [12] M. Wagemaker and F. M. Mulder, *Acc. Chem. Res.* **46**, 1206 (2013).
 [13] G. Sudant, E. Baudrin, D. Larcher, and J.-M. Tarascon, *J. Mater. Chem.* **15**, 1263 (2005).
 [14] Y.-S. Hu, L. Kienle, Y.-G. Guo, and J. Maier, *Adv. Mater.* **18**, 1421 (2006).
 [15] Y.-G. Guo, Y.-S. Hu, W. Sigle, and J. Maier, *Adv. Mater.* **19**, 2087 (2007).
 [16] M.-S. Balogun, C. Li, Y. Zeng, M. Yu, Q. Wu, M. Wu, X. Lu, and Y. Tong, *J. Power Sources* **272**, 946 (2014).
 [17] Z. Xiao, Z. Yang, L. Wang, H. Nie, M. Zhong, Q. Lai, X. Xu, L. Zhang, and S. Huang, *Adv. Mater.* **27**, 2891 (2015).
 [18] J.-Y. Hwang, H. M. Kim, S.-K. Lee, J.-H. Lee, A. Abouimrane, M. A. Khaleel, I. Belharouak, A. Manthiram, and Y.-K. Sun, *Adv. Energy Mater.* **6**, 1501480 (2016).
 [19] T. Zhou, W. Lv, J. Li, G. Zhou, Y. Zhao, S. Fan, B. Liu, B. Li, F. Kang, Q.-H. Yang, C. Zu, Y. Cui, M. R. Hill, A. F. Hollenkamp, M. Majumder, R. Zhang, G. Zhou, J. Wang, S. Fan, Y. Cui, and Y. Zhang, *Energy Environ. Sci.* **10**, 1694 (2017).
 [20] J. He, W. Zhou, X. Zhou, X. Zhong, X. Zhang, P. Wan, B. Zhu, and W. Chen, *J. Mater. Sci.: Mater. Med.* **19**, 3465 (2008).
 [21] M. Uchida, H.-M. Kim, T. Kokubo, S. Fujibayashi, and T. Nakamura, *J. Biomed. Mater. Res.* **64A**, 164 (2003).
 [22] F. J. Knorr, C. C. Mercado, and J. L. McHale, *J. Phys. Chem. C* **112**, 12786 (2008).
 [23] S. Paul and A. Choudhury, *Appl. Nanosci.* **4**, 839 (2014).
 [24] T. Okazumi, K. Ueda, K. Tajima, N. Umetsu, and T. Narushima, *J. Mater. Sci.* **46**, 2998 (2011).
 [25] C.-H. Kao, S.-W. Yeh, H.-L. Huang, D. Gan, and P. Shen, *J. Phys. Chem. C* **115**, 5648 (2011).
 [26] Y.-L. Chung, D.-S. Gan, K.-L. Ou, and S.-Y. Chiou, *J. Electrochem. Soc.* **158**, C319 (2011).
 [27] S. Andersson, *Acta Chem. Scand.* **13**, 415 (1959).
 [28] G. Kresse and J. Hafner, *Phys. Rev. B* **47**, 558 (1993).
 [29] G. Kresse and J. Hafner, *Phys. Rev. B* **49**, 14251 (1994).
 [30] G. Kresse and J. Furthmüller, *Comput. Mater. Sci.* **6**, 15 (1996).
 [31] G. Kresse and J. Furthmüller, *Phys. Rev. B* **54**, 11169 (1996).
 [32] CASM, v0.2.0 (2016). Available from <https://github.com/prisms-center/CASMcode>, doi:10.5281/zenodo.60142.
 [33] J. C. Thomas and A. Van der Ven, *Phys. Rev. B* **88**, 214111 (2013).
 [34] B. Puchala and A. Van der Ven, *Phys. Rev. B* **88**, 094108 (2013).
 [35] A. Van der Ven, J. C. Thomas, Q. Xu, and J. Bhattacharya, *Math. Comput. Simul.* **80**, 1393 (2010).
 [36] J. P. Perdew, K. Burke, and M. Ernzerhof, *Phys. Rev. Lett.* **77**, 3865 (1996).
 [37] J. P. Perdew, K. Burke, and M. Ernzerhof, *Phys. Rev. Lett.* **78**, 1396 (1997).
 [38] J. P. Perdew and A. Zunger, *Phys. Rev. B* **23**, 5048 (1981).
 [39] J. P. Perdew, J. A. Chevary, S. H. Vosko, K. A. Jackson, M. R. Pederson, D. J. Singh, and C. Fiolhais, *Phys. Rev. B* **46**, 6671 (1992).
 [40] J. P. Perdew, J. A. Chevary, S. H. Vosko, K. A. Jackson, M. R. Pederson, D. J. Singh, and C. Fiolhais, *Phys. Rev. B* **48**, 4978 (1993).
 [41] J. P. Perdew, A. Ruzsinszky, G. I. Csonka, O. A. Vydrov, G. E. Scuseria, L. A. Constantin, X. Zhou, and K. Burke, *Phys. Rev. Lett.* **100**, 136406 (2008).

- [42] J. Sun, A. Ruzsinszky, and J. P. Perdew, *Phys. Rev. Lett.* **115**, 036402 (2015).
- [43] S. L. Dudarev, G. A. Botton, S. Y. Savrasov, C. J. Humphreys, and A. P. Sutton, *Phys. Rev. B* **57**, 1505 (1998).
- [44] J. Paier, M. Marsman, K. Hummer, G. Kresse, I. C. Gerber, and J. G. Ángyán, *J. Chem. Phys.* **124**, 154709 (2006).
- [45] P. E. Blöchl, *Phys. Rev. B* **50**, 17953 (1994).
- [46] G. Kresse and D. Joubert, *Phys. Rev. B* **59**, 1758 (1999).
- [47] S. C. Abrahams, *Phys. Rev.* **130**, 2230 (1963).
- [48] A. Pearson, *J. Phys. Chem. Solids* **5**, 316 (1958).
- [49] L. K. Keys and L. N. Mulay, *Phys. Rev.* **154**, 453 (1967).
- [50] L. N. Mulay and W. J. Danley, *J. Appl. Phys.* **41**, 877 (1970).
- [51] J. M. Sanchez, F. Ducastelle, and D. Gratias, *Physica A* **128**, 334 (1984).
- [52] J. M. Sanchez, *Phys. Rev. B* **81**, 224202 (2010).
- [53] M. Asta, C. Wolverton, D. de Fontaine, and H. Dreyssé, *Phys. Rev. B* **44**, 4907 (1991).
- [54] D. D. Fontaine, *Solid State Phys.* **47**, 33 (1994).
- [55] A. Walle and G. Ceder, *J. Phase Equilib.* **23**, 348 (2002).
- [56] G. L. W. Hart, V. Blum, M. J. Walorski, and A. Zunger, *Nat. Mater.* **4**, 391 (2005).
- [57] T. Mueller and G. Ceder, *Phys. Rev. B* **80**, 024103 (2009).
- [58] L. J. Nelson, G. L. W. Hart, F. Zhou, and V. Ozoliš, *Phys. Rev. B* **87**, 035125 (2013).
- [59] See Supplemental Material at <http://link.aps.org/supplemental/10.1103/PhysRevMaterials.2.033604> for details about the coordinates of enumerated structures.
- [60] S. Andersson, B. Collén, U. Kuylenstierna, and A. Magnéli, *Acta Chem. Scand.* **11**, 1641 (1957).
- [61] B. P. Burton and A. van de Walle, *Calphad* **39**, 97 (2012).
- [62] A. V. Ruban, V. I. Baykov, B. Johansson, V. V. Dmitriev, and M. S. Blanter, *Phys. Rev. B* **82**, 134110 (2010).
- [63] M. D. Banus, T. B. Reed, and A. J. Strauss, *Phys. Rev. B* **5**, 2775 (1972).
- [64] D. Watanabé, J. R. Castles, A. Jostsons, and A. S. Malin, *Acta Crystallogr.* **23**, 307 (1967).
- [65] A. A. Valeeva, A. A. Rempel, and A. I. Gusev, *Inorg. Mater.* **37**, 603 (2001).
- [66] A. L. Kutepov and S. G. Kutepova, *Phys. Rev. B* **67**, 132102 (2003).
- [67] U. Argaman, E. Eidelstein, O. Levy, and G. Makov, *Mater. Res. Express* **2**, 016505 (2015).
- [68] E. S. Bumps, H. D. Kessler, and M. Hansen, *Trans. Am. Soc. Met.* **45**, 1008 (1953).
- [69] J. Muscat, V. Swamy, and N. M. Harrison, *Phys. Rev. B* **65**, 224112 (2002).
- [70] F. Labat, P. Baranek, C. Domain, C. Minot, and C. Adamo, *J. Chem. Phys.* **126**, 154703 (2007).
- [71] M. E. Arroyo-de Dompablo, A. Morales-García, and M. Taravillo, *J. Chem. Phys.* **135**, 054503 (2011).
- [72] Z. Hu and H. Metiu, *J. Phys. Chem. C* **115**, 5841 (2011).
- [73] J. Moellmann, S. Ehrlich, R. Tonner, and S. Grimme, *J. Phys.: Condens. Matter* **24**, 424206 (2012).
- [74] M. T. Curnan and J. R. Kitchin, *J. Phys. Chem. C* **119**, 21060 (2015).
- [75] M. Koiwa and M. Hirabayashi, *J. Phys. Soc. Jpn.* **27**, 801 (1969).
- [76] P. G. Wahlbeck and P. W. Gilles, *J. Am. Ceram. Soc.* **49**, 180 (1966).
- [77] A. Kohan, P. Tepeesch, G. Ceder, and C. Wolverton, *Comput. Mater. Sci.* **9**, 389 (1998).
- [78] A. van de Walle and M. Asta, *Model. Simul. Mater. Sci. Eng.* **10**, 521 (2002).
- [79] Q. Xu and A. Van der Ven, *Intermetallics* **17**, 319 (2009).
- [80] R. Roy and W. B. White, *J. Cryst. Growth* **13-14**, 78 (1972).
- [81] S. Yamaguchi, M. Koiwa, and M. Hirabayashi, *J. Phys. Soc. Jpn.* **21**, 2096 (1966).
- [82] S. Yamaguchi, *J. Phys. Soc. Jpn.* **27**, 155 (1969).
- [83] S. Yamaguchi, K. Hiraga, and M. Hirabayashi, *J. Phys. Soc. Jpn.* **28**, 1014 (1970).
- [84] A. Navrotsky and O. J. Kleppa, *J. Am. Ceram. Soc.* **50**, 626 (1967).
- [85] D. A. H. Hanaor and C. C. Sorrell, *J. Mater. Sci.* **46**, 855 (2011).
- [86] J. Graciani, A. Márquez, and J. F. Sanz, *Phys. Rev. B* **72**, 054117 (2005).
- [87] D. A. Andersson, P. A. Korzhavyi, and B. Johansson, *Phys. Rev. B* **71**, 144101 (2005).
- [88] J. Trail, B. Monserrat, P. López Ríos, R. Maezono, and R. J. Needs, *Phys. Rev. B* **95**, 121108 (2017).
- [89] T. Lan, C. W. Li, O. Hellman, D. S. Kim, J. A. Muñoz, H. Smith, D. L. Abernathy, and B. Fultz, *Phys. Rev. B* **92**, 054304 (2015).
- [90] S. P. Rudin, M. D. Jones, and R. C. Albers, *Phys. Rev. B* **69**, 094117 (2004).
- [91] R. J. Nicholls, N. Ni, S. Lozano-Perez, A. London, D. W. McComb, P. D. Nellist, C. R. Grovenor, C. J. Pickard, and J. R. Yates, *Adv. Eng. Mater.* **17**, 211 (2015).
- [92] M.-H. Chen, B. Puchala, and A. Van der Ven, *Calphad* **51**, 292 (2015).
- [93] B. Monserrat, N. D. Drummond, and R. J. Needs, *Phys. Rev. B* **87**, 144302 (2013).
- [94] J. C. Thomas and A. Van der Ven, *Phys. Rev. B* **90**, 224105 (2014).
- [95] J. C. Wojdel, P. Hermet, M. P. Ljungberg, P. Ghosez, and J. Íñiguez, *J. Phys.: Condens. Matter* **25**, 305401 (2013).
- [96] C. E. Patrick and K. S. Thygesen, *Phys. Rev. B* **93**, 035133 (2016).
- [97] All ground states with the exception of the the Ti_4O_7 and Ti_5O_9 Magnéli phases were predicted to be nonmagnetic for the $U = 0$ calculations. Several phases had finite magnetic moments for nonzero U values. The rocksalt based γ' -TiO, Ti_6O_7 , and Ti_2O_3 , for example, exhibited magnetic moments when $U = 3$ eV and greater. Magnéli Ti_3O_5 was found to favor a finite magnetic moment when $U = 2$ eV and greater. Corundum Ti_2O_3 was found to converge to both a nonmagnetic state and a ferromagnetic state depending on how the magnetic moments were initialized. Surprisingly the lowest energy state for U values less than or equal to 4 eV was the nonmagnetic state. All HSE calculations predicted nonmagnetic ground states.
- [98] H. Okamoto, *J. Phase Equilib. Diffusion* **19**, 89 (1998).
- [99] C. Ponticaud, A. Guillou, P. Lefort, and F. J. Worzala, *Phys. Chem. Chem. Phys.* **2**, 1709 (2000).
- [100] H. H. Wu and D. R. Trinkle, *Phys. Rev. Lett.* **107**, 045504 (2011).
- [101] J. D. Hunter, *Comput. Sci. Eng.* **9**, 90 (2007).